Journal of Wind Engineering and Industrial Aerodynamics, 41-44 (1992) 79–90
Elsevier

Lift on an Oscillating Cylinder in Smooth and Turbulent Flow

H.M. Blackburn and W.H. Melbourne

Department of Mechanical Engineering, Monash University, Clayton 3168, Australia.

Abstract

Lift forces were measured at six sections of a circular cylinder in smooth and turbulent flows over the Reynolds number range 1.1×10^5 to 5.5×10^5. Introduction of turbulence of 18% longitudinal intensity produced a return to organized vortex shedding, characterized by large lift forces with a broad spectral peak centred near $St = 0.23$. With the cylinder in forced oscillation of amplitudes up to 3% of diameter, motion-correlated forces were observed. Adaptive digital filter techniques were used to remove inertial components of force transducer signal.

1. INTRODUCTION

The prediction of amplitudes of cross wind vibration response of slender structures of circular cross section is one of the fundamental problems of Wind Engineering. Among the structures encompassed by this description are chimney stacks, masts and space-frame members. Typically, cross wind response amplitudes to vortex shedding must be limited to less than 5% of diameter in order to prevent the possibility of large amplitudes and stresses caused by lock-in effects.

For Reynolds numbers typical of structures and flows in Wind Engineering applications, vortex shedding is quasi-periodic, and prediction models are often based in random vibration theory, with estimates of mean-squared modal response amplitudes as the outcome. Models of this kind have been described by Vickery and Basu (1983), and the Engineering Sciences Data Unit in ESDU Item 85038. Both these models incorporate a description of vortex-induced lift forces on rigid cylinders in terms of the cross-spectra of lift acting at different points on the span and models of motion-correlated forces, which comprise an increasing proportion of lift force as oscillation amplitude increases. Both models give a coefficient of variation between predicted and observed response amplitudes of about 25% (Vickery & Basu 1984, ESDU 1985). A part of the variation can be attributed to a lack of data for the aerodynamic parameters which underly the models.

Only a limited amount of data are available to assist in the description of lift forces on rigid cylinders at transcritical Reynolds numbers, from a mixture of wind tunnel measurements made in smooth flows and a scattering of measurements conducted on full scale structures in turbulent flows. The extent of spanwise correlation of lift forces in transcritical flows has not been studied. In addition, the role of turbulence in establishing transcritical flows at comparatively low Reynolds numbers is poorly understood.

Motion-correlated forces referred to above are an aspect of the phenomenon of lock-in, in which it is observed that for large oscillation amplitudes, vortex shedding and structural oscillation become phase-locked, with the relative phase being a function of reduced velocity $V_r = U/fD$. At low amplitudes of oscillation it has been found that some proportion of lift force becomes correlated motion, with the remainder being uncorrelated over long

time periods (see e.g. Toebes & Ramamurthy 1967, Jones, Cincotta & Walker 1969). The consequences and nature of this partition of force into motion-correlated and uncorrelated components are poorly understood, although it has been implicit in many experiments in which lift forces on oscillating cylinders were measured.

These points served as motivation for a wind tunnel study of the local and spanwise distribution of lift force on a circular cylinder in smooth and turbulent flows ($I_{u_{max}} = 18\%$) over a range of Re up to 5.5×10^5. The model could be forced to oscillate cross flow at amplitudes up to $\pm 3\%$ of diameter, thus permitting study of the interaction of lift and motion in these flows.

2. WIND TUNNEL MODEL

2.1. Model geometry

A cylinder model was designed to suit the 2 m high, 1 m wide working section of the Monash University 450 kW wind tunnel. In a compromise between desires for high Reynolds number, low tunnel blockage and high aspect ratio, a cylinder geometry of 200 mm diameter and 900 mm length was selected, giving a blockage ratio of 10% and an aspect ratio of 4.5:1. While it is known that this combination of blockage and aspect ratio leads to over-estimates of force coefficients in smooth subcritical flow (see e.g. West & Apelt 1982), it is expected that the effect would be smaller in super- and transcritical flows, where the wake is narrower and the spanwise coherence of vortices is expected to be lower.

To minimize the effect of tunnel wall boundary layers on the measurements, large end plates were mounted 50 mm clear of the wind tunnel walls, with the cylinder spanning the 900 mm gap between them. The plates were rectangular, extending 2.5 D upstream, 4.5 D downstream of the cylinder centreline, 9 D cross flow. Since the model was designed to oscillate in the cross flow direction it was not attached to the end plates; a central supporting tube passed through holes in the end plates and the wind tunnel walls, with the clearance gap between the cylinder and the end plates sealed using synthetic fur, which allowed relative movement but prevented air flow through the gap.

The cylinder geometry is shown in figure 1, which indicates that the cylinder was constructed in segments, supported on an inner structural tube of 100 mm diameter. The thin (0.1 D axial length) cylinder segments contained lift force transducers, while the remainder were 'blank' segments that contained no instrumentation. The clearance gaps between the segments were sealed using narrow strips of 30 μm thick polyurethane elastomer, glued on. The use of six force transducers spaced along the span allowed measurements of lift force to be made simultaneously at the six locations. Since the lift transducers were narrow compared to typical lift force correlation lengths (order 1 D), the measurements obtained were assumed to be good approximations to the sectional lift forces.

2.2. Transducer construction

Transducer construction is illustrated in figure 2. The outer segments of the transducers were made as light as possible, consistent with the need for stiffness, by use of fibre composites, foamed plastics and balsa wood, giving a mass of 16 gm. Lift force was transmitted to the support cylinder by beam springs which had semi-conductor strain gauges bonded to them. The natural frequency of the outer segments on the springs was 400 Hz, well above the frequency content of the lift forces. Each transducer also contained an accelerometer for the measurement of cylinder motion and cancellation of inertial forces.

The mechanical arrangement of the springs and gauges provided sensor elements which

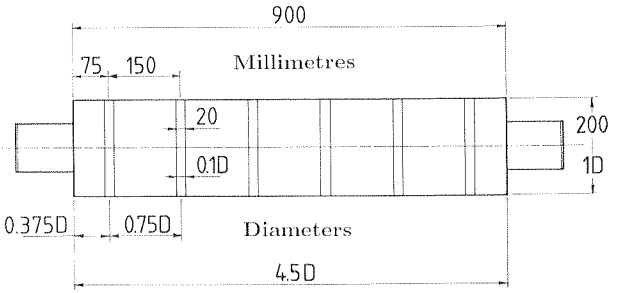

Figure 1: Cylinder geometry: six $0.1\,D/20$ mm long lift force transducers separated by 'blank' sections, all supported from an inner structural tube.

were sensitive only to lift force. Measurements showed the transducers to be about 150 times more sensitive to lift than to drag forces. The sensitivity to applied moments was also low; when cross flow force was applied at one cylinder radius from the centreline, strain bridge output changed by approximately 1/60th of the full reading obtained with the force centrally applied.

2.3. Oscillation system

The elements of the system can be seen in the sketch of figure 3. The system was designed to produce forced sinusoidal oscillations of up to $\pm 3\%\, D$ amplitude over a frequency range 10 Hz to 50 Hz. The part of the model described so far occupied the working section; outside this, it was supported and guided by a rectangular aluminium tube yoke and a harness of taut music wires which constrained motion to the cross flow direction. Underneath the tunnel floor, the yoke was clamped to two steel beam springs, and the assembly was driven at its resonant frequency by an electromagnetic shaker. The frequency could be adjusted by changing the length or section of the springs. A steel truss assembly held the shaker and the ends of the beam springs, and was clamped down to the main floor beams of the laboratory. Plenum boxes were used to surround the wire harness and the cylinder ends where they penetrated the working section walls. The yoke struts passed through the lower faces of the boxes, with a small clearance limiting the flow of air into the working section.

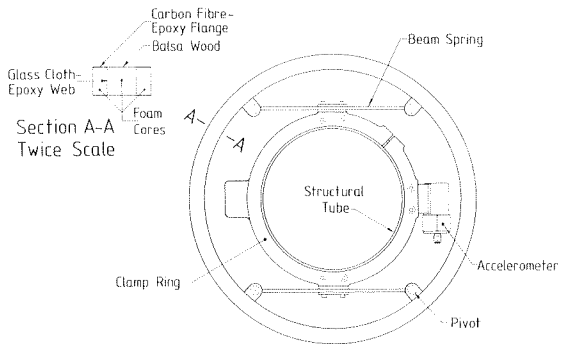

Figure 2: End view of lift force transducer station, showing construction. A full bridge of semiconductor strain gauges were bonded to the beam springs.

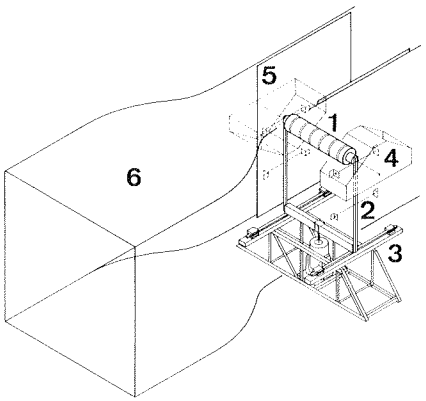

Figure 3: Sketch of cylinder installed in wind tunnel. **1**: Cylinder with six force transducers; **2**: Driving yoke and wire harness; **3**: Support truss, springs and electromagnetic shaker; **4**: Plenum box; **5**: End plate; **6**: Contraction.

3. FLOW

Five turbulence configurations were selected. Smooth flow was obtained using a combination of wire meshes and an aluminium honeycomb screen, while turbulent flow was produced using a bi-planar array of slats located upstream of the contraction. The spanwise average values of the longitudinal and transverse turbulence intensities (I_u & I_v), together with the turbulence integral length scales are shown in table 1.

Table 1: Spanwise-averaged turbulence intensities and integral scales at the model centreline position for the five flow configurations.

Configuration	I_u%	I_v%	L_u^x/D
1	18.0	14.1	0.53
2	9.6	8.7	0.53
3	4.2	4.2	0.50
4	3.6	3.6	0.25
'Smooth Flow'	0.6	0.6	0.10

The close agreement between I_u and I_v, except for the highest intensity case, indicates that the turbulence was approaching isotropy after distortion caused by the contraction. For Configuration 1, differing longitudinal and transverse intensities (I_u = 18%, I_v = 14%) indicate that the turbulence was still approaching isotropy, but it was felt that the high values, similar to those found in many full scale applications, made its inclusion worthwhile.

Turbulence integral scales L_u^x were obtained by fitting von Kármán spectra to the measured velocity spectra.

4. SIGNAL PROCESSING

Signals from the transducers (six accelerometers, six strain bridge amplifiers) were low-pass filtered, then digitized and stored on magnetic tape using a minicomputer. All subsequent signal processing was carried out digitally.

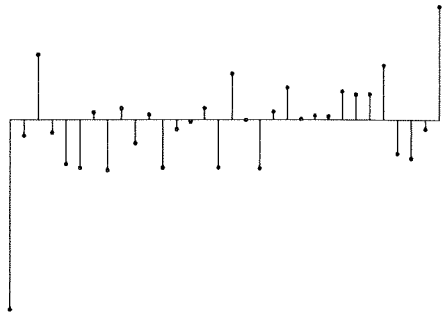

Figure 4: Typical impulse response function of a digital filter used for cancellation of inertial signal.

4.1. Inertial signal cancellation

When the cylinder was oscillating, forces due to the mass and acceleration of the transducer outer segments were produced, in addition to aerodynamic forces. Adaptive digital filter techniques described by Bellanger (1987) were used to identify the relationship between accelerometer outputs and strain bridge signals found when the cylinder was forced to oscillate without flow. An example of a digital filter produced by this technique is illustrated in figure 4. To remove the inertial component of force transducer output in the presence of flow, the accelerometer signals were convolved with the digital filters and the result subtracted from the total force transducer signals, leaving aerodynamic forces as residual. An example of force transducer signal before and after removal of inertial force component is shown in figure 5.

To check the accuracy of the cancellation method, tests were run in which data for both the identification and measurement phases were recorded without flow. The removal of inertial signal typically left a residual with RMS magnitude less than one analogue to digital conversion level (5 mV). When flow was applied, the typical RMS level of the aerodynamic force signal was 0.5 V, giving a signal to noise ratio of approximately 40 dB.

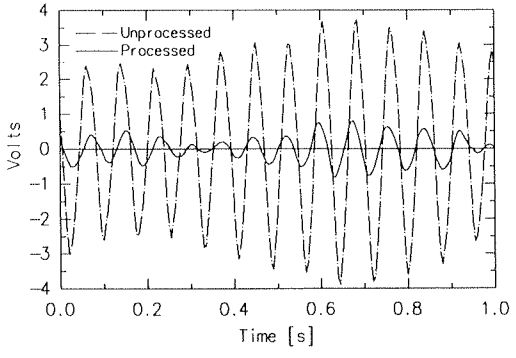

Figure 5: Example of transducer signal obtained in smooth subcritical flow, before and after removal of inertial signal component.

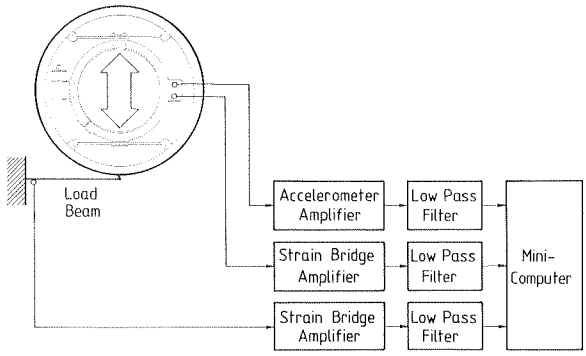

Figure 6: Schematic of equipment set-up for dynamic calibration of force transducer. Transducer forced to oscillate cross flow while in contact with load beam.

4.2. Re-introduction of 'added mass' forces

Although the cancellation system effectively removed all forces due to the acceleration of the transducer segment mass, it is known from both theory (Milne-Thomson 1960) and measurements (Lundgren et al. 1979) that 'added mass' forces per unit length equivalent to accelerating the mass per unit length of one cylinder's cross-section of fluid exist at small oscillation amplitudes in still fluid. These forces were also cancelled using the system described above, so forces of the appropriate magnitude were subsequently calculated with the aid of the accelerometer timeseries, and added back to the force transducer signals. While viscous forces proportional to cylinder velocity must also have arisen when the cylinder oscillated in still fluid, it can be shown with the use of theoretical results for oscillatory boundary layers (Batchelor 1967) that at the cylinder Reynolds numbers for oscillation in still fluid, the resulting viscous forces were small enough to lie within the noise level of the measurements, and so were ignored.

4.3. Integration of accelerometer timeseries

Since both velocity and acceleration of the cylinder were required for subsequent analysis of results, the cylinder acceleration timeseries were integrated to obtain velocity timeseries. In order to avoid phase errors inherent in typical numerical integration formulae, a numerical integration procedure was devised in which DFT coefficients were manipulated in the frequency domain (effectively by dividing them by $j2\pi f$). Data were then returned to the time domain for further processing.

4.4. Dynamic calibration

It was found that the polyurethane film used to seal the clearance gaps between the transducer and 'blank' cylinder segments had slightly viscoelastic properties. Upon application of a steady load to a transducer, strain bridge amplifier output would jump nearly instantaneously to about 90% of its full value, then relax slowly to the full value over a period of several minutes. It was established experimentally that over the frequency range of interest (5 Hz to 150 Hz), the effect was almost purely elastic.

In response, a dynamic calibration procedure was devised. The layout of the equipment is illustrated in figure 6. The method relied on applying a fluctuating force to the force

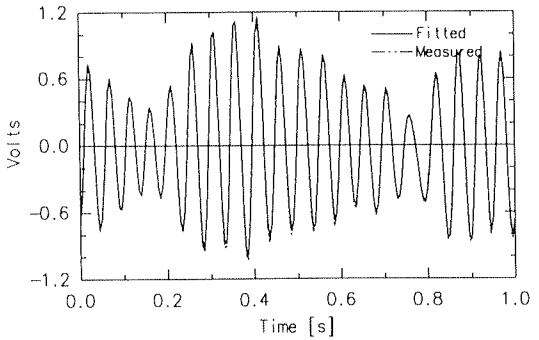

Figure 7: Dynamic calibration: after removal of inertial signal, amplitude of residual transducer output was fitted to match measured load beam signal.

transducer segment, using a pre-calibrated lightweight steel load beam.

Calibration proceeded as follows. First, the model was forced to oscillate without the load beam, and data collected from the transducer strain gauge bridge and accelerometer amplifiers. These data were used to identify the digital filter which related acceleration and inertial transducer response. Then the load beam was pre-loaded against the transducer segment with sufficient deflection that it would not lose contact when the cylinder was oscillated. The cylinder was forced to oscillate again, and outputs from the three amplifiers (load beam and transducer strain bridges, transducer accelerometer) were recorded. Next, the inertial component of force transducer output was estimated by convolution of the digital filter with the accelerometer signal, and subtracted to leave a remainder due to the force applied by the load beam. Finally, this remainder was scaled to match the load beam signal using a least-squares fit. The resulting scale factor was multiplied by the load beam force-voltage calibration factor to produce a calibration for the transducer strain bridge.

Advantages of the method were that it provided a cross-check on the inertial signal removal technique, and enabled the force measurement procedure to be checked under simulated experimental conditions. An example of part of the calibration procedure is shown in figure 7, where the fitted residual transducer signal is shown with the signal from the load beam.

5. RESULTS

5.1. Plan of experiments

It was decided to first carry out a series of experiments in which the model was held fixed and the range of achievable Reynolds numbers was traversed for each of the five flow configurations.

With the oscillation system described above, it was possible to vary the Reynolds number $Re = UD/\nu$ and the reduced velocity $V_r = U/fD$ independently, since the frequency of oscillation could be readily changed. Traverses of reduced velocity ($3 < V_r < 6$) were carried out at each end of the Reynolds number envelope ($1.1 \times 10^5 < Re < 5.5 \times 10^5$) with the aim of studying the interaction of motion and lift both in smooth subcritical flow and in turbulent transcritical flows. Amplitudes $\alpha = y_{\max}/D = 1\%$, 2% and 3% were used.

Due to uncertainty about blockage correction at these Reynolds numbers, none was applied.

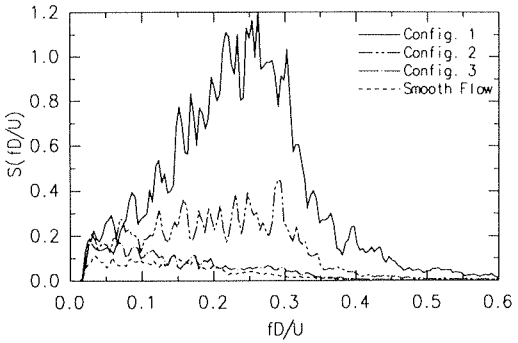

Figure 8: Influence of turbulence configuration on sectional lift force spectra at $Re \approx 4.6 \times 10^5$. Spectra are normalized such that their areas equal the mean-squared coefficients of sectional lift force.

5.2. Effect of turbulence

With the cylinder held fixed in smooth flow, it was found that the critical transition occurred at $Re \approx 2.3 \times 10^5$. At higher Reynolds numbers, no distinct peak was observed in the lift force spectra, with spectral densities decreasing monotonically from maxima at low frequencies.

Introduction of low intensity turbulence (Configs. 3 & 4) produced critical transition at lower Reynolds numbers, as expected. Above transition, lift force spectra and variances were very similar to those observed in smooth flow.

For the two highest turbulence intensities (Configs. 1 & 2), critical transition occurred at Reynolds numbers below the minimum attainable in the experiment. for each intensity, there was only a comparatively slight change in properties of lift with Reynolds number over the range investigated. The change in properties of lift with turbulence intensity, however, was pronounced. At the highest intensity ($I_u = 18\%$), a clear but very broad peak existed in the lift force spectra, centred around $St = fD/U = 0.23$. RMS sectional lift was approximately three times greater than in smooth flow. In addition, the spanwise correlation of lift increased above that in the supercritical flows at lower Reynolds numbers. The second highest intensity produced results between those for the lower intensities and the highest, with intermediate RMS sectional lift and some evidence of a peak in the lift force spectra.

The influence of turbulence intensity is clearly shown in the comparison of spectra of sectional lift for four of the five turbulence configurations, all recorded at $Re \approx 4.6 \times 10^5$, presented in figure 8.

5.3. Motion-correlated forces in subcritical smooth flow

When the cylinder was forced to oscillate cross flow, it was found, as in other experiments (e.g. Toebes & Ramamurthy 1967, Jones, Cincotta & Walker 1969) that some proportion of lift force could be correlated with cylinder motion over extended time periods. In this experiment, the amount of force correlated with motion was estimated by extracting least-squares fits of lift force timeseries to cylinder acceleration and velocity timeseries. The residual force timeseries was thus uncorrelated with motion on a least-squares basis. This processing is the digital equivalent of analogue procedures which have been applied in the past, for example by Jones, Cincotta and Walker. An example of this process is shown in figure 9, where the decomposition just described is illustrated, with velocity- and acceleration-correlated force timeseries extracted from the total to leave a residual uncorrelated timeseries of lift coefficient.

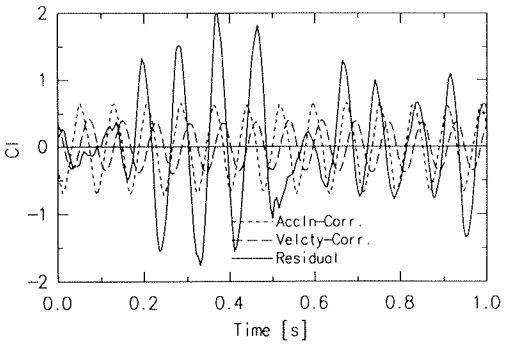

Figure 9: Sectional coefficient of lift in smooth subcritical flow decomposed into parts equivalent to the long-time-average acceleration- and velocity-correlated forces, with residual uncorrelated force.

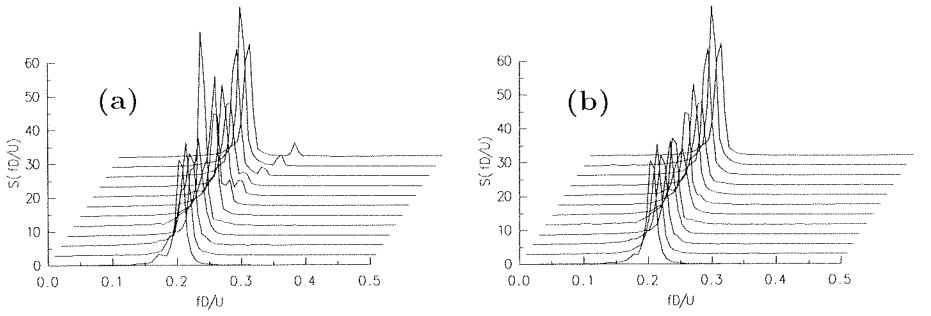

Figure 10: Spectra of sectional lift forces in smooth subcritical flow, showing the relative contribution of motion-correlated forces with the cylinder oscillating near the critical reduced velocity, with amplitude $\alpha = 3\%$. **a**: Spectra prior to extraction of motion correlated force components; **b**: Spectra of residual forces.

Lift spectra An examination of the spectra of total lift forces shows that two peaks are often visible, one at the frequency of cylinder oscillation, the other at the Strouhal frequency (fig. 10 (a)). After extraction of motion-correlated terms from the timeseries of force, the associated spectra reveal that the peaks at the cylinder oscillation frequencies have been removed (fig. 10 (b)). It can be seen, as for the timeseries of lift in figure 9, that the motion-correlated lift makes only a small contribution to the total lift force at these amplitudes of motion.

Force coefficients The motion-correlated coefficients of lift extracted by the procedure described above have been converted to force coefficients C_a and K_a for the acceleration- and velocity-correlated lift respectively. In these forms they are more directly comparable with structural mass and damping.

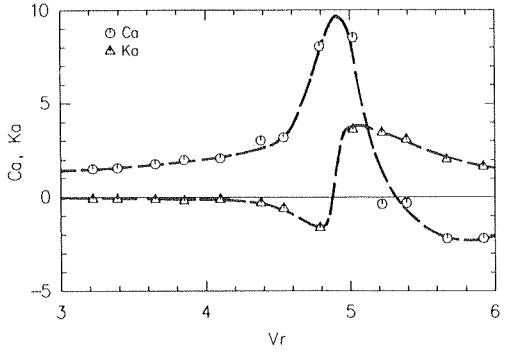

Figure 11: Variation with reduced velocity V_r of coefficients C_a and K_a of motion-correlated forces in smooth subcritical flow. $Re \approx 1.6 \times 10^5$, $\alpha \approx 3\%$.

The *coefficient of added mass*, C_a, describes the acceleration-correlated force per unit length, l_a, as a proportion of the force per unit length required to accelerate the mass of fluid displaced by the cylinder:

$$l_a = -C_a \cdot \rho \frac{\pi D^2}{4} \cdot \ddot{y}$$

The velocity-correlated force per unit length, l_v, is described in terms of an *aerodynamic damping parameter*, K_a.

$$l_v = K_a \cdot 16f \cdot \rho \frac{\pi D^2}{4} \cdot \dot{y}$$

Here, the term $K_a \cdot 16f \cdot \rho\pi D^2/4$ has the same dimensions and form as a coefficient of structural damping per unit length. For convenience of comparison, an equivalent structural damping ratio can be computed; for a uniform cylinder with mass per unit length m, oscillating with a uniform mode shape,

$$\zeta_{\text{aero}} = -K_a \frac{\rho D^2}{m}$$

The variation in smooth subcritical flow of C_a and K_a with reduced velocity V_r for $\alpha = 3\%$ is shown in figure 11. The rapid variation of C_a and K_a near the critical reduced velocity $V_r \approx 5$ is apparent; this represents a change in phase angle of the motion-correlated forces with respect to cylinder motion.

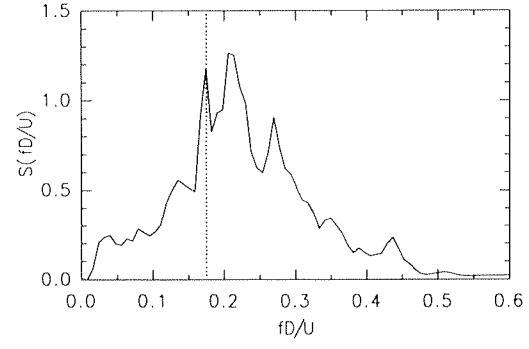

Figure 12: Spectrum of sectional lift with cylinder oscillating in turbulent flow (config. 1, $I_u = 18\%$); $Re \approx 4.6 \times 10^5$, $\alpha \approx 3\%$. Dotted line indicates frequency of oscillation.

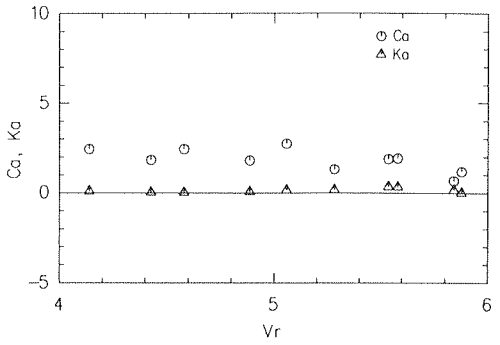

Figure 13: Variation with reduced velocity V_r of coefficients C_a and K_a of motion-correlated forces in turbulent transcritical flow, $I_u = 18\%$. $Re \approx 4.6 \times 10^5$, $\alpha \approx 2\%$.

5.4. Motion-correlated forces in transcritical turbulent flow

Motion-correlated forced were observed for all Reynolds numbers and flow configurations, but in general the magnitudes were smaller than in subcritical smooth flow, and the magnitudes and phases with respect to motion of the forces showed more scatter and little influence of reduced velocity.

An example of a lift force spectrum from one transducer in the $I_u = 18\%$ turbulence configuration with $Re = 4.6 \times 10^5$ is shown in figure 12, while the variation of C_a and K_a with V_r for this flow are given in figure 13.

6. DISCUSSION

As has been known for many decades, smooth flows with Reynolds numbers in the range available in this experiment ($1.1 \times 10^5 < Re < 5.5 \times 10^5$), produce both subcritical and supercritical behaviour, while introduction of turbulence brings about the critical transition at lower Reynolds numbers. It has been anticipated that turbulence would also promote the appearance of transcritical flow at lower Reynolds numbers than in smooth flow (see e.g. Zdravkovich 1990). The results presented here for the two highest turbulence intensities support this view; in particular the lift force spectrum for $I_u = 18\%$, which has a broad spectral peak centred at $St = 0.23$, indicates that strong vortex shedding was re-established at $Re = 4.6 \times 10^5$, despite the disruptive influence of turbulence.

The measurements of lift on the oscillating cylinder in subcritical smooth flow show similar characteristics to previous measurements obtained in smooth flows. The rapid variation in motion-correlated force near the critical velocity is probably associated with a change in phase of motion-correlated vortex shedding with respect to cylinder motion, as indicated by previous flow-visualization experiments (see Zdravkovich 1982). It should be emphasized that the force coefficients for motion-correlated forces represent time-averaged values and do not imply, as may be suggested by figure 9, that steadily-fluctuating motion-correlated forces exist during each cycle of cylinder motion.

The measurements of motion-correlated forces obtained in turbulent transcritical flow are significant for the design of full scale structures in Wind Engineering applications. The scatter in the results probably reflects the fact that vortex shedding was less well-organized than for the subcritical smooth flow. The absence of any clear trend of motion-correlated forces with V_r is also likely to be a reflection of this lack of organization. Average values of motion-correlated force coefficients suggest that long-time-average values are likely to be small in these flows. Taken overall, the results for $I_u = 18\%$, $Re = 4.6 \times 10^5$ suggested slight positive values for K_a, of order 0.2.

7. CONCLUSIONS

In many experiments in which the objective is to measure loads on oscillating structures, it is necessary to cancel out transducer signals which are caused by motion of the structure, so that fluid-induced forces or pressures may be analysed separately. Adaptive digital filter techniques were shown to be well suited to the task.

On the evidence of a broad but well-defined peak in the spectra of lift force, high intensity turbulence promoted transition to transcritical flow at Reynolds numbers which would produce supercritical behaviour in smooth flow. The broadness of the peak reflects the fact that vortex shedding was poorly organized when compared to smooth subcritical and transcritical flows.

Introduction of forced cross-flow oscillation produced motion-correlated lift forces. In smooth subcritical flow, variation of these forces with reduced velocity was similar to that observed in previous experiments, with rapid variation near the critical reduced velocity. Examination of the spectra of lift force produced before and after removal of motion-correlated forces showed that removal of motion-correlated forces also removed spectral peaks at frequencies of cylinder oscillation.

Motion-correlated forces in transcritical turbulent flows showed a good deal of scatter and small average values.

8. REFERENCES

Batchelor, G.K., 1967, *An Introduction to Fluid Dynamics*, Cambridge University Press.

Bellanger, M., 1987, *Adaptive Digital Filters and Signal Analysis*, Marcel Dekker.

Engineering Sciences Data Unit, 1985, *Item 85038: Circular-Cylindrical Structures: Dynamic Response to vortex shedding. Pt. 1: Calculation Procedures and Derivation.*

Jones, G.W., Cincotta, J.J. & Walker, R.W., 1969, 'Aerodynamic forces on a stationary and oscillating cylinder at high Reynolds numbers', *NASA TR R-300.*

Lundgren, H., Brink-Kjær, O., Sand, S.E. & Jacobsen, V., 1979, 'Improved physical basis of wave forces', *ASCE Proc. Spec. Conf. Civ. Eng. in Oceans IV*, Vol. 1., San Francisco.

Milne-Thomson, L.M., 1960, *Theoretical Hydrodynamics*, 4th ed., MacMillan.

Toebes, G.H., & Ramamurthy, A.S., 1967, 'Fluidelastic forces on circular cylinders', *ASCE J Eng. Mech. Div.*, EM6, pp. 1–20.

Vickery, B.J., & Basu, R.I., 1983, 'Across-wind vibration of structures of circular cross section. Pt. 1: Development of a mathematical model for two-dimensional conditions', *J Wind Eng. Ind. Aero.*, **12**, pp. 49–73.

Vickery, B.J., & Basu, R.I., 1984, 'The response of reinforced concrete chimneys to vortex shedding', *Eng. Struct.*, **6**, pp. 324–333.

West, G.S., & Apelt, C.J., 1982, 'The effects of tunnel blockage and aspect ratio on the mean flow past a circular cylinder with Reynolds numbers between 10^4 and 10^5', *J Fluid Mech.*, **114**, pp. 361–377.

Zdravkovich, M.M., 1982, 'Modification of vortex shedding in the synchronization range', *ASME J Fluids Eng.*, **104**, pp. 513–517.

Zdravkovich, M.M., 1990, 'Conceptual overview of laminar and turbulent flows past smooth and rough circular cylinders', *J Wind Eng. Ind. Aero.*, **33**, pp. 53–62.